Pharm Res (2014) 31:1930–1937
DOI 10.1007/s11095-013-1294-y

RESEARCH PAPER

High Resolution Visualization and Analysis of Nasal Spray Drug Delivery

Kiao Inthavong • Man Chiu Fung • Xuwen Tong • William Yang • Jiyuan Tu

Received: 10 September 2013 / Accepted: 31 December 2013 / Published online: 19 February 2014

ABSTRACT

Purpose Effective nasal drug delivery of new-generation systemic drugs requires efficient devices that can achieve targeted drug delivery. It has been established that droplet size, spray plume, and droplet velocity are major contributors to drug deposition. Continual effort is needed to better understand and characterise the physical mechanisms underpinning droplet formation from nasal spray devices.

Methods High speed laser photography combined with an in-house designed automated actuation system, and a highly precise traversing unit, measurements and images magnified in small field-of-view regions within the spray was performed.

Results The qualitative results showed a swirling liquid sheet at the near-nozzle region as the liquid is discharged before ligaments of fluid are separated off the liquid sheet. Droplets are formed and continue to deform as they travel downstream at velocities of up to 20 m/s. Increase in actuation pressure produces more rapid atomization and discharge time where finer droplets are produced.

Conclusions The results suggest that device designs should consider reducing droplet inertia to penetrate the nasal valve region, but find a way to deposit in the main nasal passage and not escape through to the lungs.

KEY WORDS atomization · droplet size · droplet velocity · nasal spray · spray plume

Electronic supplementary material The online version of this article (doi:10.1007/s11095-013-1294-y) contains supplementary material, which is available to authorized users.

K. Inthavong · M. C. Fung · X. Tong · J. Tu (✉)
School of Aerospace, Mechanical and Manufacturing Engineering
RMIT University, PO Box 71, Bundoora, VIC 3083, Australia
e-mail: jiyuan.tu@rmit.edu.au

W. Yang
CSIRO Process Science and Engineering, Clayton South, VIC, Australia

INTRODUCTION

The need to develop new and innovative drug delivery systems is crucial for improved patient compliance, cost-effectiveness, and reduction of systemic side effects. The nasal route for delivery of new vaccines is an attractive proposition due to the possibility of obtaining a systemic and local response (1–3). However a number of spray deposition studies *in-vivo* (4,5), *in-vitro* (6), and computational (7,8) have found spray droplets producing high deposition in the anterior half of the nasal cavity. Based on the inertial property theory (9), droplet size, and velocity are implicated for the high deposition.

The nasal cavity is an extremely complex anatomy with its primary function to humidify and filter foreign aerosols from the inhaled air before it reaches the lungs, and not for delivering drugs to the main nasal passage. The nasal anatomy exhibits narrow passageways highlighted by the anterior nasal valve region. This triangular valve-like region has the smallest cross-sectional area located approximately 2–3 cm from the nostril inlet (10) and acts as a flow limiting region (3) before expanding into the main nasal passage. The mucus lining surfaces help to trap larger aerosols that are unable to navigate through the narrow passageways, and mucociliary clearance removes these aerosols via the gastrointestinal tract or by manual forced effort. These conditions present a hostile environment for drug delivery into the main nasal passage where rapid absorption across the mucosa into the blood stream can occur (Fig. 1).

The aqueous spray pump is the dominant delivery device in the nasal drug delivery market (11) which relies on an actuation force to atomize the drug formulation as it is discharged from the device. The underlying objective of the device is to deliver sufficient drug formulation to the target site, attributed to many factors. Kundoor and Dalby (12) evaluated the effect of formulation and administration-related variables and found that the deposition area decreased

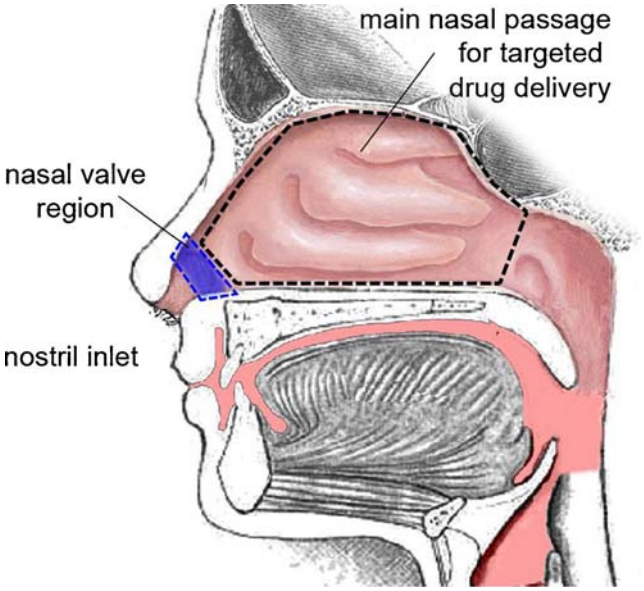

Fig. 1 Schematic of nasal cavity showing region for targeted drug delivery for absorption through the mucosa and into the blood stream.

with increasing viscosity but this was mediated by an increase in droplet size and a narrowing of the spray plume. Foo *et al.* (13) found that insertion angle and plume angle are critical factors in determining deposition efficiency and this was confirmed by a number of computational simulations (8,14,15). Cheng *et al.* (16) evaluated four nasal spray pumps and found that spray plume and droplet size distribution were important factors in deposition. Based on these studies if a spray device can produce a combination of desirable spray characteristics (e.g. spray plume, viscosity, insertion angle, droplet size distribution) then more efficient drug delivery systems can be produced.

Assessment of the different spray characteristics and factors associated with the spray device itself is critical for a better understanding of effective device design. Guo and Doub (17) characterised the droplet velocity and droplet size distribution and found that the stroke length of the internal spray device and actuation velocity had an impact on droplet size distribution and spray plume geometry. Dayal *et al.* (18) measured the droplet size distributions influenced by formulation viscosity while Doughty *et al.* (19) and Kippax *et al.* (20) investigated the influence of actuation force. In a series of studies by Fung *et al.* (21,22), both the external spray characteristics and droplet size distributions were measured which revealed three main phases of spray development (pre-stable, stable, and post-stable), each of which produced varying droplet size distributions.

In a continuing effort to better understand and characterise the physical behaviour of nasal spray development, this paper presents for the first time, high resolution images of spray atomization, and detailed velocity and droplet size distributions. Measurements are taken at different moments during atomization and at 11 locations given that the parameters vary spatially and temporally. Unlike previous studies that use Laser Doppler Anemometry, high speed laser image photography is used to capture the fast moving spray in high resolution to reveal the mechanisms in nasal spray development.

METHODS

An in automated actuation system was developed by the authors, that used a pneumatic actuator with a two-way solenoid valve controlled by a programmable logic control (PLC) (Fig. 2). The spray bottle used is a commercially available nasal spray device kindly provided by Glaxo Smith Kline, capable of delivering 200 sprays per bottle with 50 mcg of formulation per actuation claimed by the pharmaceutical company for normal operation. A back pressure is supplied by the pressure mains and is adjustable by a pressure regulator. In the experiment, the pressure was set as 2.05, 2.45 and 2.65 bar, representing a typical range of hand operation by adults. The whole system is placed on a traverse unit, so it can be manoeuvred with high precision (+/−17 μm) to a desired location for measurement.

The high speed photography used a Particle/Droplet Image Analyser (PDIA) system that included a New Wave 120 mJ double-pulsed Nd:YAG laser with a SensiCam 12-bit digital charge-coupled device (CCD) camera (1,280× 1,024 pixels). The spray images were captured with long-distance micro-scope lens with magnification of 2.23 to achieve a physical size field-of-view (FOV) of 3.85 mm× 3.08 mm with resolution of 3.01 μm/pixel. This means that to capture the complete spray plume in the near nozzle region, 11 FOV regions are required. Figure 3 shows the FOVs where each row (R) is labelled, from R1 (closest to the spray orifice) to

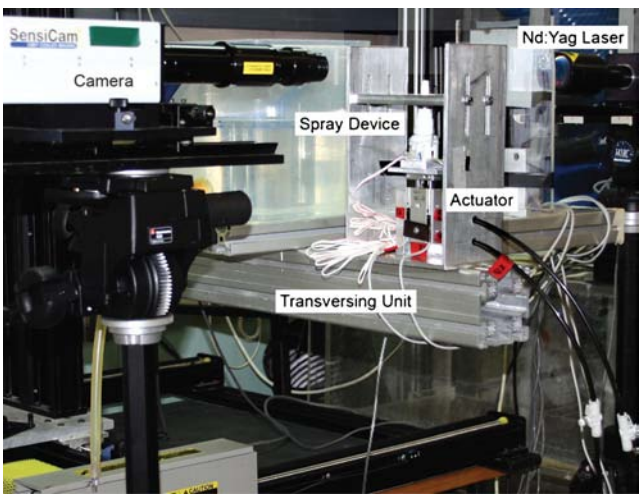

Fig. 2 Experimental setup of the high speed photography using a Particle/Droplet Image Analyser system.

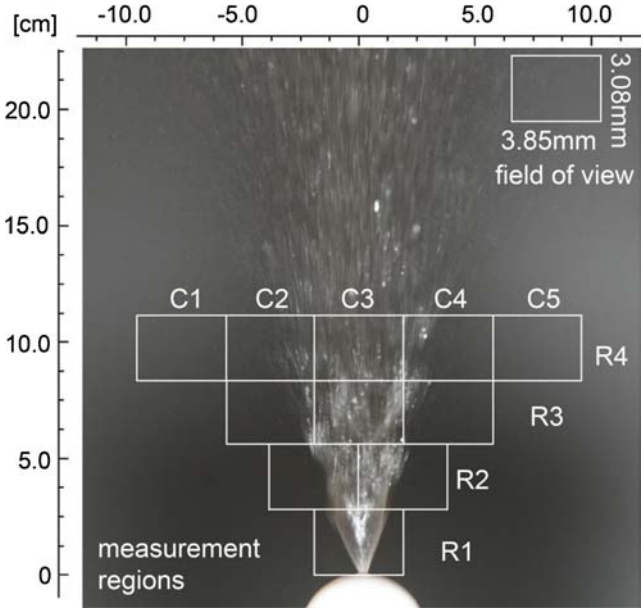

Fig. 3 Field of View (FOV) regions used for analysis of the spray in the near nozzle region.

R4 (furthest distance from the spray orifice), while each column (C) is labelled from C1 to C5 from left to right for rows R3, and R4.

The PDIA system captures two images sequentially separated by 6 μs. Velocities are calculated based on the displacement of each droplet from the paired images, divided by 6 μs. To achieve sufficient statistical average a set of 100 image pairs for each FOV region and at three different moments in time was obtained. The PDIA system detects each droplet and its diameter by an automated segmentation threshold algorithm located on the focal plane (23). Further details of the image processing and droplet analysis has been reported by the authors earlier in Inthavong *et al.* (24).

RESULTS

Spray Plume Development

The spray plume development within the first 3 mm of the spray nozzle during one actuation cycle for a 2.05Bar case is shown in Fig. 4. In this region the spray first develops into a tulip shape before expanding into a cone as a liquid sheet and no droplets are formed at all. This implies that droplet formation occurs further downstream and that this has influence on a user's insertion angle and depth as to where the droplets will first form inside the nasal cavity. The liquid sheet swirls

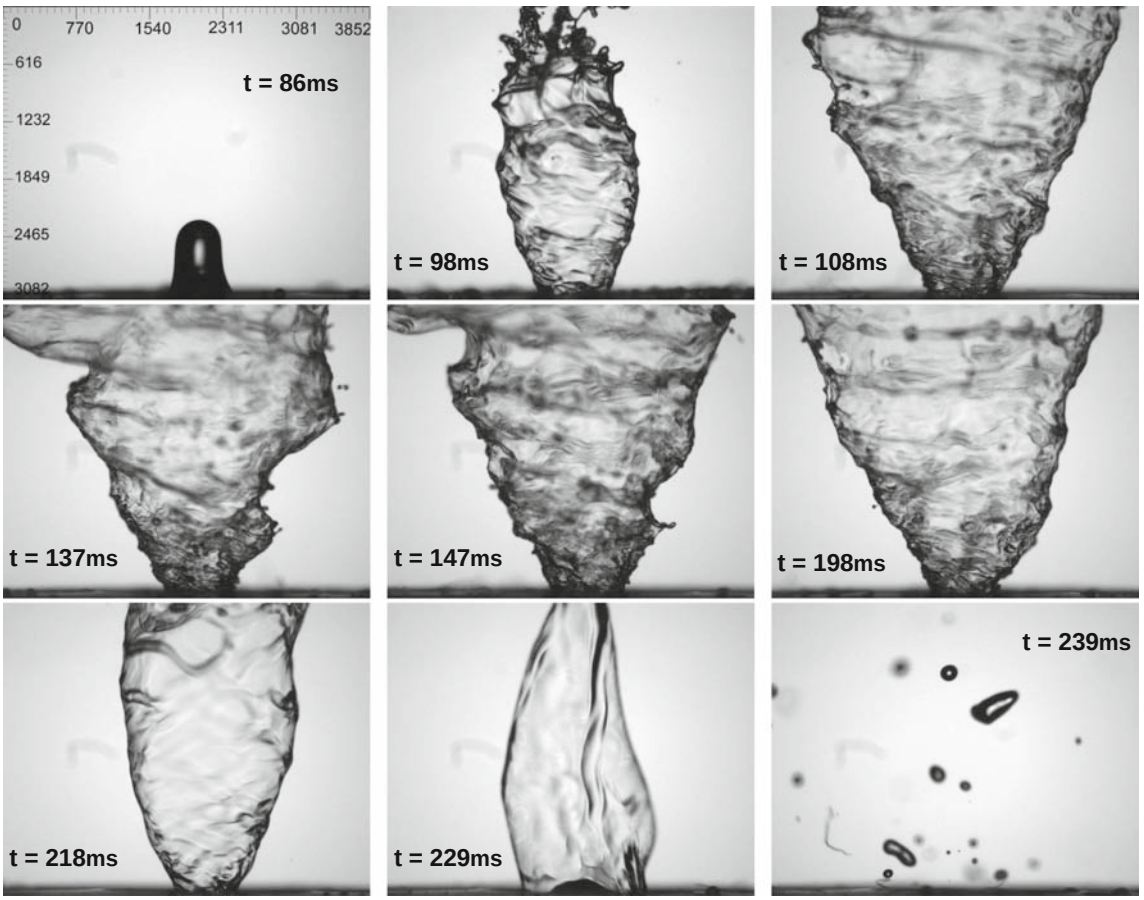

Fig. 4 Spray atomization development at 2.05Bar taken at region R1. The timing first begins from the moment actuation begins.

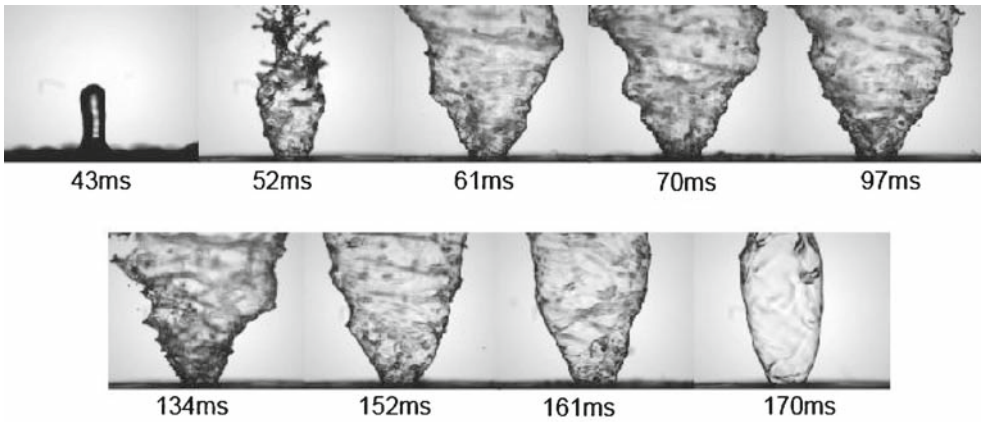

(a) 2.45 Bar

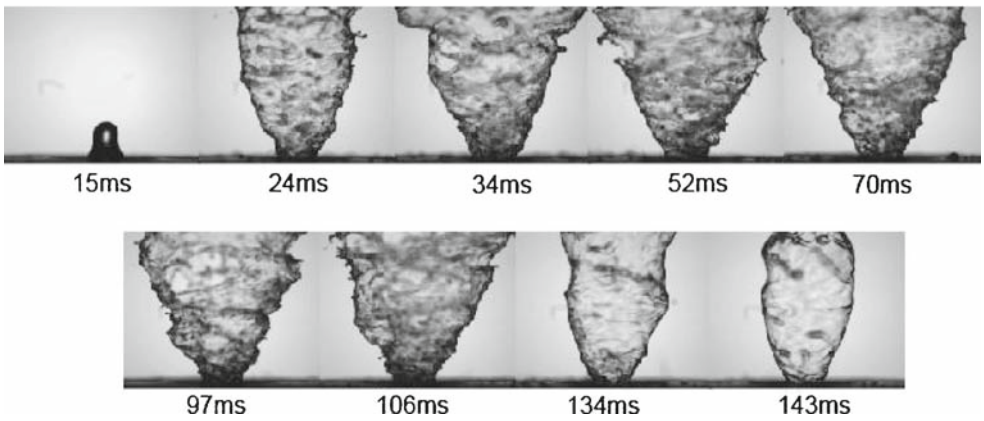

(b) 2.65 Bar

Fig. 5 Spray atomization development profiles at (**a**) 2.45Bar and (**b**) 2.65Bar taken at region R1. The timing first begins from the moment actuation begins.

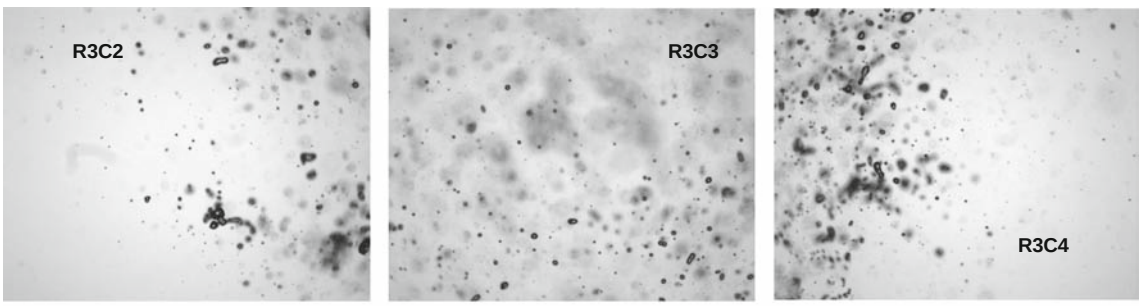

(a) Row R3

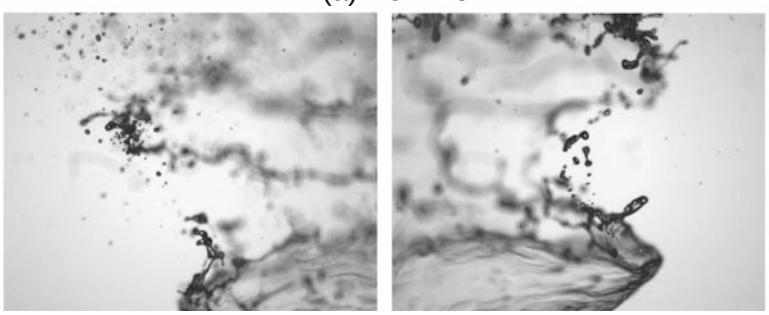

(b) Row R2, left and right

Fig. 6 Spray images in each of the FOV regions within (**a**) Row 3 and (**b**) Row 2.

violently from the actuation force before collapsing as the liquid finishes discharging. For actuation pressures of 2.45 and 2.65 Bar the images showed qualitatively similar liquid sheet development but the actuation cycle is completed in successively quicker time with increasing pressure (Fig. 5). Spray atomization duration for each pressure case are 2.05Bar–229 ms, 2.45Bar–170 ms, 2.65–150 ms. There is a slight delay between the beginning of actuation and the instance at which the liquid formulation first discharges because of the force required to overcome the internal atomizer. The total spray discharge times are: 2.05Bar–144 ms, 2.45Bar–129 ms, 2.65–127 ms.

Downstream from the nozzle in row R2, the liquid sheet breaks up into ligaments before atomizing into droplets. Figure 6b shows the droplets forming around the rim of the liquid sheet as it begins to disintegrate into droplets. The swirling nature can also be visualized in the ripples along the surface of the liquid sheet. Established droplets found in Row R3 (Fig. 6a) show that the shapes are not necessarily spherical given the continual deformation as the droplets move through the quiescent surrounding air. The FOV, R3 is at a distance of 6.16 mm to 9.24 mm from the nozzle, while its width is 11 mm from the spray centre, which is of similar order to the dimensions of the anterior nasal cavity. The continual droplet deformation can lead to secondary breakup where the droplets breakup into subsequent smaller droplets (25). The images found in row R4 are similar to that of row R3, and therefore are not shown for brevity.

Droplet Size Distribution

Droplet size distribution measurements, by volume mean diameter, are taken at two different times during actuation, t_1=126 ms, t_2=168 ms for 2.05Bar case and t_1=88 ms and t_2=134 ms for 2.65Bar case (Fig. 7) and these instances of time can be referenced with spray development by the images in Figs. 4 and 5. The central FOV columns, C2, C3, and C4 along rows R3 and R4 are given. The general shape of the

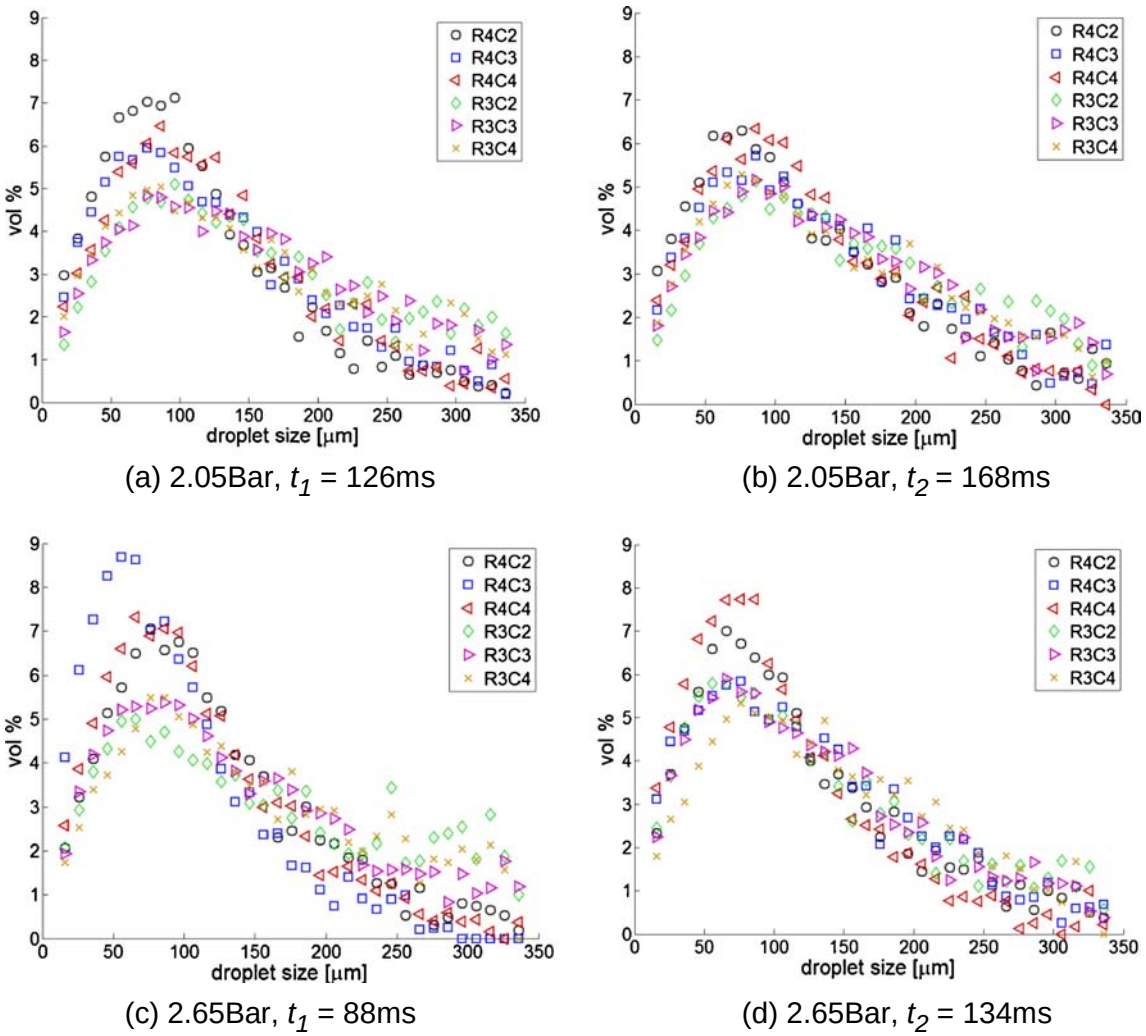

Fig. 7 Droplet size distributions of the volume mean diameters obtained for six FOVs along the rows R3, and R4 at (**a**) 2.05Bar, t_1 = 126 ms (**b**) 2.05Bar, t_2 = 168 ms, (**c**) 2.65Bar, t_1 = 88 ms and (**d**) 2.65Bar, t_2 = 134 ms.

droplet size distribution is a skewed distribution with a peak ranging between 50 μm and 110 μm. Comparisons between each of the FOVs shows some disparities. A larger percentage of finer droplets are found in row R4 and this is particularly more significant for the higher actuation pressure case. Overall the 2.65Bar case produced a skewed distribution towards the left which means that a larger percentage of finer droplets are produced.

Droplet Velocity

Droplet velocities were obtained from two sequential snapshots separated by 6 μs in time. Two sample image pairs in Fig. 8 with grid spacing of 337 μm show the droplets' trajectory and its velocity determined through the distance of its trajectory over the period of time. The droplets in subregion R2-right contain streaks of liquid ligaments, which are present due to the liquid separating from the liquid sheet as it forms droplets for the first time. Subsequently droplets can be seen deforming and rotating as it moves further downstream. This suggests the droplet size is dynamic and has potential to further atomize or shatter upon deposition on the mucosal surface of the nasal cavity.

The average droplet velocity across the spray width for each of the FOV regions along rows R3 and R4 are shown in Fig. 9. For a low actuation pressure of 2.05Bar, a parabolic velocity profile is found with peak velocities occurring in the middle regions of the spray while at the spray periphery, low velocities occur. In contrast the velocity profile remains relatively constant around 21 m/s across the width of the spray, for an actuation pressure of 2.65Bar.

DISCUSSION

An understanding of the physical mechanisms underlying the atomization process from a nasal spray device can reveal important information leading to more effective device design. The atomization period is in the order of 150–200 ms, approximately 10% of a light inhalation breath with period of 2 s

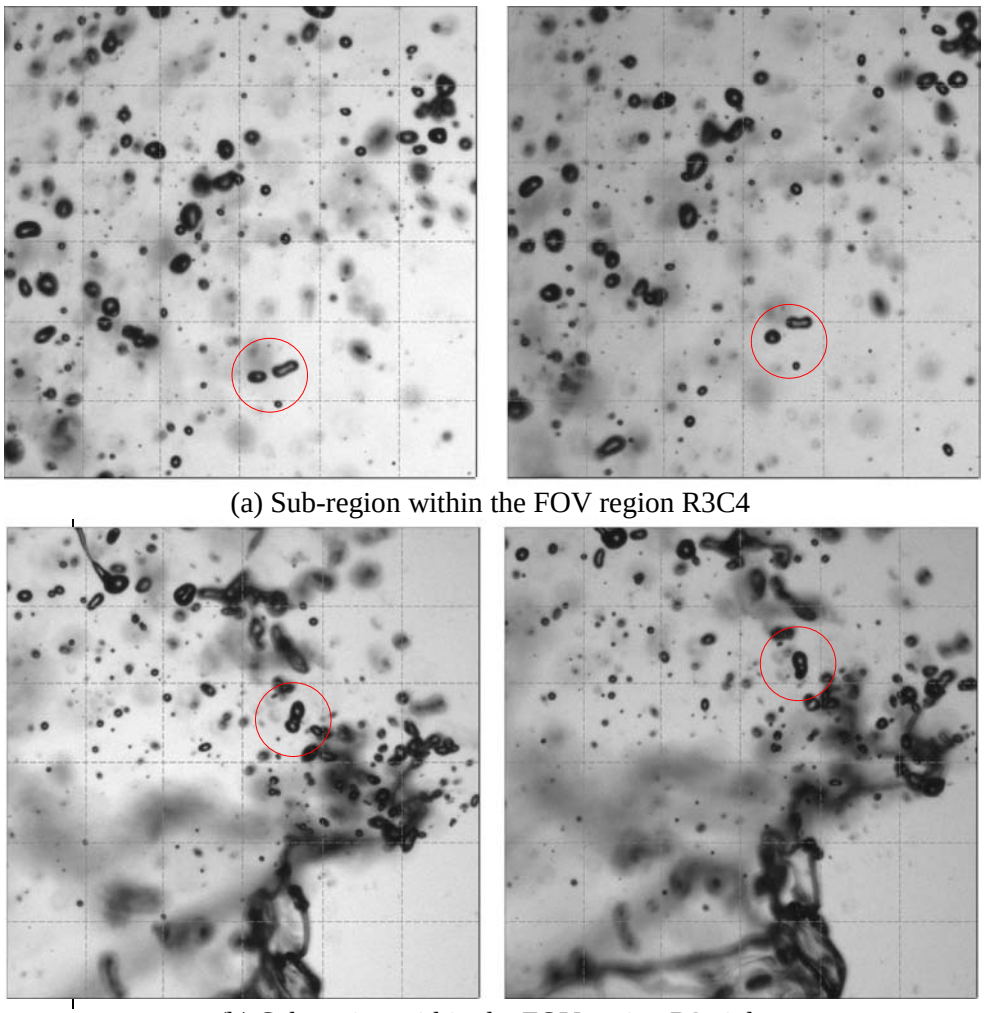

(a) Sub-region within the FOV region R3C4

(b) Sub-region within the FOV region R2-right

Fig. 8 Spray images in sub-regions within the FOV regions (**a**) R3C4 and (**b**) R2-right. Each image is separated by 6 μs in time. The initial image is brighter than the latter as the influence of the flash diminishes over the short period of time. Each square grid is 337 μm microns in size. The highlighted circle is an example of tracking individual droplets and its trajectory between the paired images.

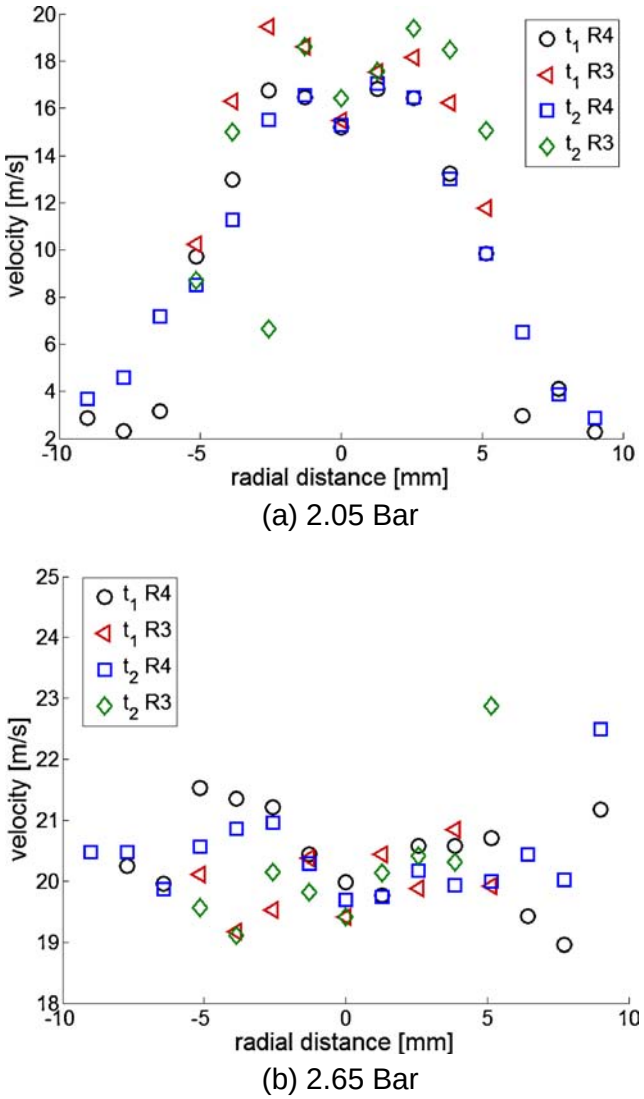

Fig. 9 Averaged droplet velocity across the rows R3 and R4, taken at (**a**) 2.05Bar for $t_1 = 126$ ms and, $t_2 = 168$ ms, (**b**) 2.65Bar, $t_1 = 88$ ms, $t_2 = 134$ ms.

(26). This means that unless the inhalation is quite extreme, then a user's breathing profile is insufficient to have an influence on the droplets. This is reinforced by the average droplet velocity reaching up to 20 m/s, which compares with a steady inhalation breathing at 20 L/min achieving velocities in the order of 0–4 m/s (14).

The images show the presence of a liquid sheet in the near nozzle, up to 6.5 mm from the nozzle. Droplets are therefore produced at a short distance from the nozzle, referred to as the break-up length, in an annulus structure or hollow cone rather than a solid spray cone. At this break-up length the droplets are at its largest diameters (along with streaks of liquid ligaments), since further downstream it secondary break-up occurs and finer droplets are formed. This suggests that spray nozzle orientation and location within the nasal cavity is important as the large droplets with high velocities exhibit greater momentum and tend to move in a trajectory aligned with the spay device orientation. The narrow passageway of the nasal cavity makes impaction a high probability for inertial dominant droplets.

Interestingly there is a variation in the droplet velocities across the radial distance in the spray plume for the 2.05Bar actuation pressure, while the increased actuation effort for the 2.65Bar produces greater velocities but overall smaller droplet sizes. Swirl chambers inside atomizers can be reconfigured to produce greater swirl thereby reducing the inertial property in the aligned velocity direction (e.g. its axial coordinate), and at the same time produce finer droplets. The nebulizer pumps traditionally used for oral delivery is well known to produce lower velocities and finer droplets and it is these properties that may be the primary cause for deposition beyond the anterior nasal cavity by nebulizers compared with spray (6)—although these finer droplets increase lung deposition, and are ideal for pulmonary drug delivery, not nasal drug delivery.

Given the high velocities and large droplet formation in the near nozzle from hand actuated spray pumps, new device designs are needed to overcome these barriers to reduce droplet deposition by inertial impaction in the anterior nasal cavity. The reduction of droplet inertia is most sensitive to droplet diameter since the inertia is proportional to the square of droplet size multiplied by the air flow velocity, $\propto d^2 U$. This reduction causes the droplets to trace or follow the air flow streamlines more readily enhancing the transport through the nasal valve. On the downside, if the droplets become too small, then the droplets follow the airflow paths too faithfully, leading to deep lung deposition—ineffective for nasal drug delivery but critically important for pulmonary drug delivery of powder formulations.

To overcome the problem of low inertial droplets entering the lungs, a recent design called the Optinose Bi-Directional™ nasal spray device requires the user to exhale into a mouthpiece which causes the soft palate to elevate and close off the nasal cavity from the pharynx, thereby producing a closed loop between one nasal chamber and the other (3). Atomized droplets that penetrate the nasal valve region then have to navigate through both chambers thereby increasing the exposure to the nasal walls for deposition.

In summary, traditional mechanical nasal spray devices deliver drug droplets that need to penetrate the narrow triangular-shaped nasal valve region to target sites of the nasal mucosa or the olfactory nerves. An optimum design would deliver droplets through the narrow nasal valve region, and then induce disturbances in the flow streamlines to enable these droplets to deposit in the main nasal passage surfaces. This remains a challenging prospect for the industry. A novel design in the Optinose Bi-Directional™ device (3) provides one solution; while CFD studies have shown that droplet diameters in the order of nanoparticles can induce more dispersed droplet deposition throughout the entire nasal

cavity, due to the increased Brownian diffusion behavior (27). At this stage atomization of a liquid spray by mechanical means cannot produce such fine droplets. Further complicating this is the agglomeration of nanoparticles, which tend to increase the droplet sizes back up to 100 nm to 1 μm. A further alternative is to decrease droplet size through increased actuation effort but this comes with higher droplet velocities—however if the liquid swirl could be increased then the droplet inertia energy can be transferred from its linear component into the radial and tangential components.

CONCLUSION

Using high speed laser photography this paper presents high resolution imaging of the spray formation from a nasal spray device to provide greater insight into the physical mechanisms of spray atomization. Increasing actuation pressure produces more rapid atomization and discharge time where finer droplets are produced. The qualitative results showed that device designs should consider reducing droplet inertia to penetrate the nasal valve region, but find a way to deposit in the main nasal passage and not escape through to the lungs.

ACKNOWLEDGMENTS AND DISCLOSURES

The authors would like to gratefully acknowledge the financial support provided by the Australian Research Council (project ID: DP120103958). The authors declare that no conflicts of interest exists regarding the publication of a manuscript.

REFERENCES

1. Ting T-Y, Gonda I, Gipps E. Microparticles of polyvinyl alcohol for nasal delivery. I. Generation by spray-drying and spray-desolvation. Pharm Res. 1992;9:1330–5.
2. Illum L. Nasal drug delviery: new developments and strategies. Drug Discov Today. 2002;7:1184–9.
3. Djupesland P. Nasal drug delivery devices: characteristics and performance in a clinical perspective—a review. Drug Deliv Transl Res. 2013;3:42–62.
4. Newman SP, Moren F, Clarke SW. Deposition pattern of nasal sprays in man. Rhinology. 1998;26:111–120.
5. Bergstrom M, Cass LR, Valind S, Westerberg G, Lundberg E-L, Gray S, *et al.* Deposition and disposition of [11C]Zanamivir following administration as an intranasal spray. Clin Pharmacokinet. 1999;36:33–9.
6. Suman JD, Laube BL, Dalby R. Comparison of nasal deposition and clearance of aerosol generated by nebulizer and an aqueous spray pump. Pharm Res. 1999;16:1648–52.
7. Inthavong K, Ge Q, Se CMK, Yang W, Tu JY. Simulation of sprayed particle deposition in a human nasal cavity including a nasal spray device. J Aerosol Sci. 2011;42:100–13.
8. Kimbell JS, Segal RA, Asgharian B, Wong BA, Schroeter JD, Southall JP, *et al.* Characterization of deposition from nasal spray devices using a computational fluid dynamics model of the human nasal passages. J Aerosol Med. 2007;20:59–74.
9. Schroeter JD, Garcia GJM, Kimbell JS. Effects of surface smoothness on inertial particle deposition in human nasal models. J Aerosol Sci. 2011;42:52–63.
10. Cole P. The four components of the nasal valve. Am J Rhinol. 2003;17:107–10.
11. Kundoorand V, Dalby RN. Assessment of nasal spray deposition pattern in a silicone human nose model using a color-based method. Pharm Res. 2010;27:30–6.
12. Kundoorand V, Dalby RN. Effect of formulation- and administration-related variables on deposition pattern of nasal spray pumps evaluated using a nasal cast. Pharm Res. 2011;28:1895–904.
13. Foo MY, Cheng YS, Su WC, Donovan MD. The influence of spray properties on intranasal deposition. J Aerosol Medic Off J Int Soc Aerosols Med. 2007;20:495–508.
14. Inthavong K, Tian ZF, Li HF, Tu JY, Yang W, Xue CL, *et al.* A numerical study of spray particle deposition in a human nasal cavity. Aerosol Sci Technol. 2006;40:1034–45.
15. Frank DO, Kimbell JS, Pawar S, Rhee JS. Effects of anatomy and particle size on nasal sprays and nebulizers. Otolaryngol Head Neck Surg. 2012;146:313–9.
16. Cheng YS, Holmes TD, Gao J, Guilmette RA, Li S, Surakitbanharn Y, *et al.* Characterization of nasal spray pumps and deposition pattern in a replica of the human nasal airway. J Aerosol Med. 2001;14:267–80.
17. Guoand C, Doub WH. The influence of actuation parameters on in vitro testing of nasal spray products. J Pharm Sci. 2006;95:2029–40.
18. Dayal P, Shaik MS, Singh M. Evaluation of different parameters that affect droplet-size distribution from nasal sprays using the Malvern Spraytec. J Pharm Sci. 2004;93:1725–42.
19. Doughty DV, Vibbert C, Kewalramani A, Bollinger ME, Dalby RN. Automated actuation of nasal spray products: determination and comparison of adult and pediatric settings. Drug Dev Ind Pharm. 2011;37:359–66.
20. Kippax PG, Krarup H, Suman JD. Applications for droplet sizing - manual versus automated actuation of nasal sprays. Pharm Technol. 2000;30–39.
21. Fung MC, Inthavong K, Yang W, Lappas P, Tu J. External characteristics of unsteady spray atomization from a nasal spray device. J Pharm Sci. 2013;3:1024–35.
22. Fung MC, Inthavong K, Yang W, Tu J. CFD modeling of spray atomization for a nasal spray device. Aerosol Sci Technol. 2012;46:1219–26.
23. Whybrew A, Nicholls TR, Boaler JJ, Booth HJ. Diode lasers-a cost effective tool for simultaneous visualisation, sizing, and velocity measurements of sprays, *Proc 15th Annual Conference on Liquid Atomization and Spray Systems*, Toulouse, France, 1999.
24. Inthavong K, Yang W, Fung MC, Tu JY. External and near-nozzle spray characteristics of a continuous spray atomized from a nasal spray device. Aerosol Sci Technol. 2012;46:165–77.
25. Lefebvre AH. Atomization and sprays. New York: Hemisphere Publishing Corporation; 1989.
26. Ishikawa S, Nakayama T, Watanabe M, Matsuzawa T. Visualization of flow resistance in physiological nasal respiration: analysis of velocity and vorticities using numerical simulation. Arch Otolaryngol Head Neck Surg. 2006;132:1203–9.
27. Ge QJ, Inthavong K, Tu JY. Local deposition fractions of ultrafine particles in a human nasal-sinus cavity CFD model. Inhal Toxicol. 2012;24:492–505.